Eur. Phys. J. Special Topics **213**, 77–102 (2012)

DOI: 10.1140/epjst/e2012-01665-4

THE EUROPEAN PHYSICAL JOURNAL SPECIAL TOPICS

Review

Unravelling low lying phonons and vibrations of carbon nanostructures: The contribution of inelastic and quasi-elastic neutron scattering

S. Rols[1,a], C. Bousige[1,2], J. Cambedouzou[2,b], P. Launois[2], J.-L. Sauvajol[3], H. Schober[1], V.N. Agafonov[4], V.A. Davydov[5], and J. Ollivier[1]

[1] Institut Laue Langevin, 38042 Grenoble Cedex 9, France
[2] Laboratoire de Physique des Solides, UMR CNRS 8502, Université Paris-Sud, 91405 Orsay, France
[3] Laboratoire Charles Coulomb, UMR 5221, Université Montpellier 2, 34095 Montpellier, France
[4] Laboratoire d'Électrodynamique des Matériaux Avancés, UMR CNRS-CEA 6157, Université François Rabelais, 37200 Tours, France
[5] L. F. Vereshchagin Institute for High Pressure Physics of the RAS, Troitsk, Moscow region, 142190, Russia

Received 27 June 2012 / Received in final form 27 September 2012
Published online 3 December 2012

Abstract. We illustrate the contribution of inelastic neutron scattering to the understanding of the vibrations and lattice excitations of fullerenes and carbon nanotubes, through some significant experimental results. Particular emphasis is placed on the study of intra and inter-molecular modes of fullerene C_{60}, as well as on the order/disorder transition characteristic of these molecules. In addition, a significant part of this article is dedicated to various intercalation compounds of fullerenes and carbon nanotubes, such as the co-crystal "fullerene-cubane" consisting of an arrangement of molecules of spherical and cubic shapes, or the compound called "peapods", in which fullerene C_{60} are inserted inside carbon nanotubes.

1 Introduction

1.1 Some historical facts

Until 1985, carbon was essentially known under two distinct allotropes: graphite and diamond (see Fig. 1). These materials, although both constituted exclusively of carbon atoms, show significantly different physical properties. For example, graphite is black and crumbly (it is used for pencils), while diamond is transparent and stands as a reference material for its hardness. These different physical properties reflect

[a] e-mail: rols@ill.eu
[b] *Present address:* Institut de Chimie Séparative de Marcoule, UMR 5257, 30207 Bagnols-sur-Ceze, France.

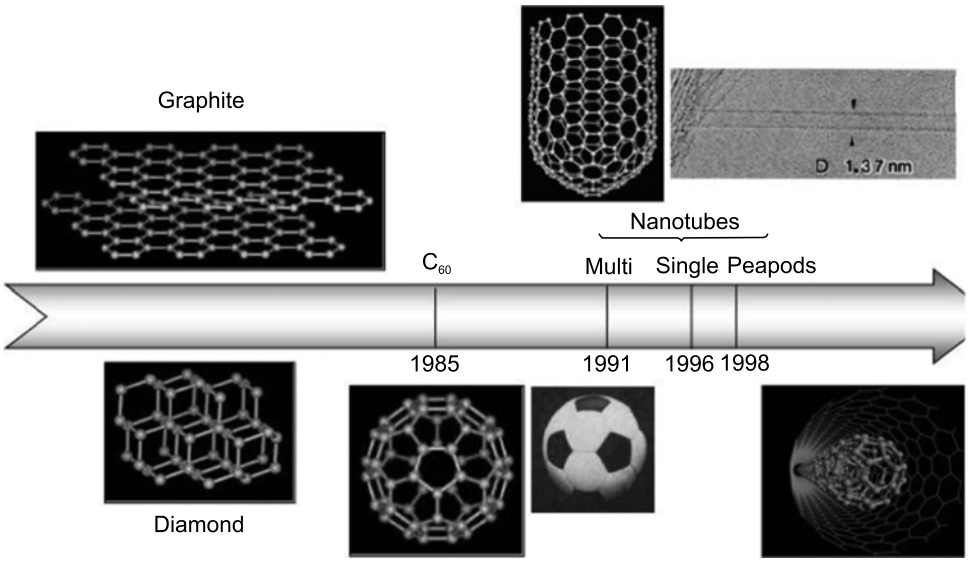

Fig. 1. Evolution of the carbon molecule family in the history.

the difference in the crystal structures of these compounds. Graphite is formed of planes in which the carbon atoms are strongly bonded by covalent interactions (sp2 hybridization), but those planes are kept packed by weak van der Waals forces, resulting in the brittleness of this material at macroscopic scale. In the case of diamond, carbon atoms are bonded by strong covalent interactions (sp3 hybridization) in such a way that each carbon atom is at the center of a tetrahedron of carbon atoms. To a macroscopic scale, such a structure results in a high hardness. During an experiment aiming at reproducing interstellar conditions for the synthesis of molecules, H. Kroto, R.F. Curl and R.E. Smalley [1] identified a new molecule made up exclusively of carbon: the fullerene C_{60}, which can be regarded as a third allotropic form of carbon.

Fullerenes C_{60} molecules are unique because they retain a very high symmetry despite the large number of atoms that compose them. We can describe the structure of a C_{60} as the assembly of 60 carbon atoms located at the vertices of a truncated icosahedron (see Fig. 2). A C_{60} has 32 faces distributed into 12 pentagons and 20 hexagons, just like a "classic" football[1], and 90 edges. This particular structure has inspired the name of the molecule, which was baptized fullerene in honor of the architect Richard Buckminster Fuller, designer of the geodesic dome erected on the pavilion of the United States at the World Exhibition in Montreal in 1967.

Other carbon cage-type molecular structures were synthesized, and are also called fullerenes. We find among them the ovoidal fullerene C_{70}. To study and understand the physical properties of these new molecules, many attempts to synthesize them in large quantities were made. It was during one of them, in 1991, while using the method of the electric arc, that S. Iijima[2] identified carbon nanotubes for the first time [2].

[1] The "Teamgeist" balloon-type that appeared in 2006 replaced these balls in official competitions. These new balls have only 14 faces.

[2] Oberlin et al. (J. Cryst. Growth **32** (3), 335 (1976)) had in fact observed carbon nanotubes 15 years before, but no response from the scientific community followed their discovery.

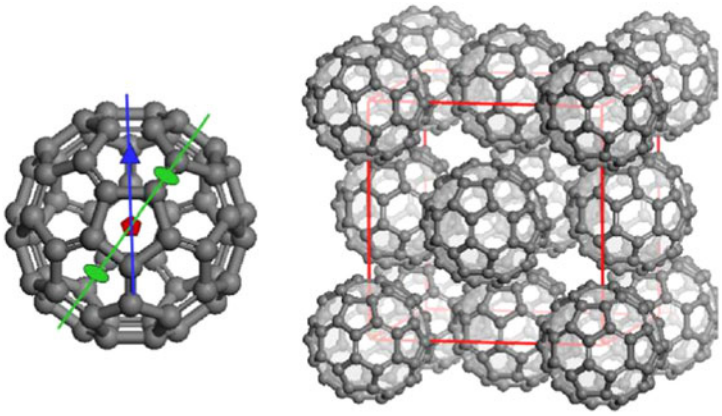

Fig. 2. *Left*: schematic view of a fullerene C_{60}. A five-fold symmetry axis (pentagon), a three-fold symmetry axis (triangle) and a two-fold symmetry axis (oval) are shown. – *Right*: each C_{60} molecule is located at a site in the FCC cell. Note that the identical orientation of the molecules in that figure doesn't correspond to any of the stable crystal phase (nor $Fm\bar{3}m$, or $Pa\bar{3}$).

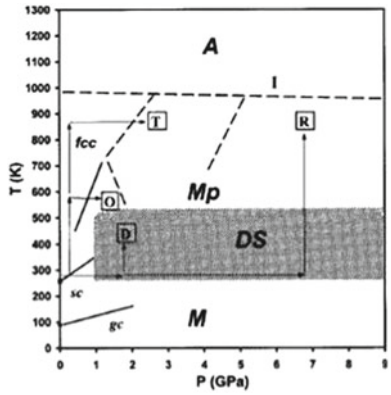

Fig. 3. Temperature and Pressure (T,P) phase diagram of fullerene C_{60}. A, Mp, DS and M stands for the amorphous, polymeric, dimeric and monomeric forms of C_{60} respectively. From ref. [3].

1.2 Scope and organization of the review

Fullerenes are often used to illustrate physical concepts related to molecular crystals. Indeed, their very high symmetry provides physicists with educational systems, the most studied and most widely used being the famous fullerene C_{60}. In addition, these compounds possess a rich phase diagram, where polymeric compounds can be synthesized under specific conditions of pressure, temperature and/or doping (see phase diagram in Fig. 3). These polymer phases are formed from the arrangement of cages connected by covalent bridges. Depending on the number of covalent bonds per molecule, the cages undergo different deformations and their supramolecular structure changes. The molecular crystal stiffens and its character becomes gradually closer to that of an atomic crystal.

In this review, we aim at illustrating the contribution of inelastic neutron scattering techniques to the study of the low lying excitations associated with carbon molecular crystal. We therefore discuss in the very first part of this paper the vibrational

dynamics of fullerene C_{60} as a textbook molecular crystal in three dimensions. We will then highlight the modifications of the lattice dynamics when guest molecules are inserted inside the octahedral voids of the cubic lattice and how this affects the C_{60} phase diagram. We will thereafter discuss the dynamics of single-walled carbon nanotubes organized into bundles. Finally, we will present the results of the study of the dynamics of nano-systems resulting from the perfect match between the diameters of C_{60} and that of carbon nanotubes: the nano-peas or "peapods", which are composed of 1D chains of C_{60} confined inside nanotubes.

2 The vibrations of a three-dimensional molecular crystal: The fullerene C_{60} in its solid phase and its insertion compounds

2.1 Pure C_{60} crystal

2.1.1 Structure, symmetry and the "order-disorder" transition

The icosahedral symmetry of C_{60} implies the presence of various elements of symmetry. In terms of symmetry axes, there are 6 axes of order 5 that connect the centers of two opposite pentagons, 10 axes of order 3 that connect the centers of two opposite hexagons, and finally 15 2-fold axes that connect the two midpoints of two opposite double bonds. An example of each of these axes is given in Fig. 2. Finally, two types of chemical bonds ensure the cohesion of the molecule: there are 60 single bonds shared by a hexagon and an adjacent pentagon, and 30 double bonds common to two adjacent hexagons.

In their crystalline phase, C_{60} molecules are organized on a 3D lattice and interact through weak van der Waals forces. Subjected to certain treatments at high pressure and high temperature (HPHT) they can also form covalent bonds, leading to interconnected networks. Figure 3 shows a phase diagram published by V. Davydov et al. in 2000 [3]. We refer the reader interested in the precise meaning of the various domains to the original article. In this chapter we will focus our attention to the areas marked fcc, sc and gc which refer to domains in the phase diagram where the lattice structure of a C_{60} crystal is respectively "face centered cubic", "simple cubic" and "glass".

At ambient temperature and pressure, the C_{60} molecules are in a plastic crystal phase in which they are animated by quasi-free, isotropic, rotational motions. This structure can be described using the space group $Fm\bar{3}m$, the molecules cristallizing on a face-centered cubic lattice (fcc) with unit cell parameter 14.15 Å. The rapid, almost isotropic, reorientations in the disordered phase ($T > 260\,K$) have been studied by experimental techniques such as nuclear magnetic resonance [6], X-ray diffuse scattering [7] and quasi-elastic neutron scattering [8]. If temperature is lowered below $T_c \simeq 260\,K$, the crystal undergoes a first order transition to an "ordered" phase in which the C_{60} remain located at the same crystallographic sites, but no longer possess rotational movement. Their rotational diffusion is blocked, and the ordering of their orientations lowers the symmetry of the lattice.

The ordered structure can be described within the space group $Pa\bar{3}$. However, the relative orientations between adjacent molecules can still fluctuate between two distinct orientations denoted H and P (see Fig. 4), whose respective populations are temperature dependent. For temperatures below 90 K, there is an orientational freezing below which molecules C_{60} remain fixed in their orientations. The C_{60} is then in a state of "orientational glass". We will call in the following "ordered phase" the simple cubic phase ($T < 260\,K$), on the clear understanding that a certain amount of orientational disorder still persists in this phase.

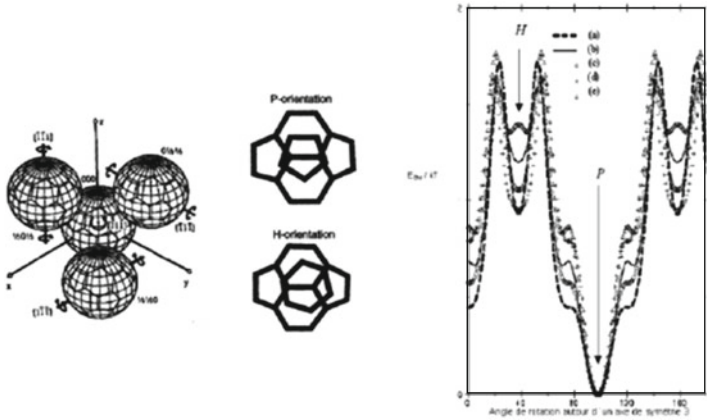

Fig. 4. *Left*: schematic representation of the C_{60} orientations in their ordered phase (space group $Pa\bar{3}$) – *Middle*: orientation of a C_{60} with respect to a pentagon or a hexagon of the neighboring molecule according to its orientation "P" or "H". From ref. [4] – *Right*: orientational energy potential depending on the angle of rotation around an axis of order 3. According to ref. [5].

2.1.2 Lattice dynamics in the ordered phase ($T < 260\,K$)

The major characteristic of a molecular crystal is the important difference between the values of the – large – intramolecular force constants (*i.e.* characteristics of the covalent bonding between atoms of the same molecule) and softer intermolecular ones. This results in a decoupling of the movements of the carbon atoms at the surface of a molecule (intra-molecular vibrations) with respects to that of the whole molecule (rotations, translations of the molecule). In the case of C_{60}, this results in a very clear separation between the bands at low energy ($E < 10\,meV$), characteristic of the lattice modes, from those within the molecules, called "molecular", and located at higher energy ($E > 25\,meV$). While the lattice modes (phonons, librations) do not involve any deformation of the C_{60} cage, molecular vibrations involve periodic deformations of their shape. These different energy ranges are separated by a band which is usually called gap. In bulk C_{60}, the latter extends over an energy range of more than 20 meV.

Molecular vibrations

A C_{60} molecule has 174 molecular modes. The icosahedral symmetry of the molecule requires that a large number of these modes are degenerate. In the end, only 46 distinct frequencies can be measured[3]. The modes can be grouped according to the following decomposition in irreducible representations:

$$2A_g + A_u + 3T_g^1 + 4T_u^1 + 4T_g^2 + 5T_u^2 + 6G_g + 6G_u + 8H_g + 7H_u. \qquad (1)$$

Of these 46 modes, only 4 are infrared active, and 10 are active in Raman spectroscopy. The other 32 vibrational modes can then be studied using inelastic neutron scattering (INS).

The first INS measurements were performed on powders of C_{60}, thus giving access to the generalized density of states (GDOS) of vibrational modes. The first experimental determination of the GDOS of a powder of fullerene C_{60} was done by

[3] We often call a "mode" all degenerate modes of the same frequency.

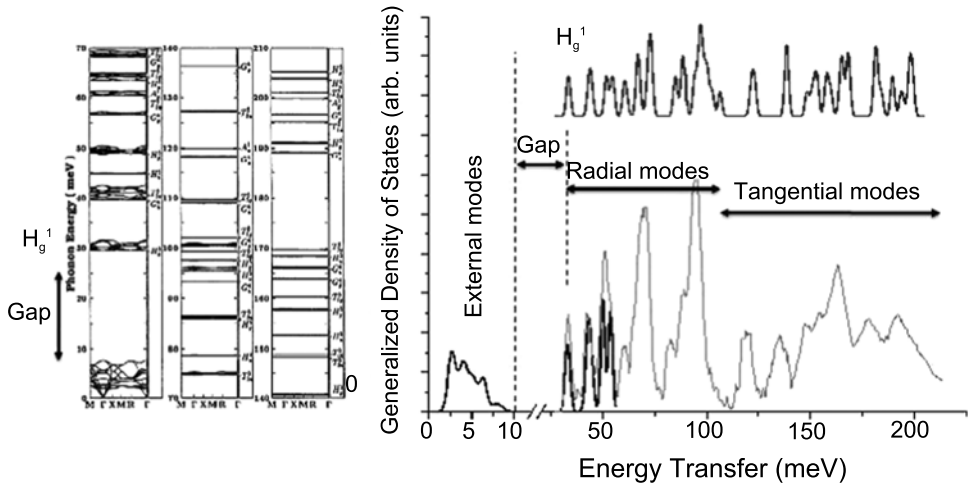

Fig. 5. *Left*: dispersion curves calculated by lattice dynamics of a C_{60} crystal (from ref. [9]). – *Right*: phonon density of states of a C_{60} crystal measured on IN4C (black) and IN1BeF (grey) at the ILL. Experimental data are compared to DFT calculations with an isolated C_{60} molecule (inset). The first Hg^1 intramolecular mode of the C_{60} is marked, as well as the gap zone (see text).

Capelletti et al. at the NIST (Washington) [10], using a filter-analyzer spectrometer. They were followed by measurements performed the following year at ISIS (Oxford), using the time of flight spectrometer filter-analyzer TFXA, by Coulombeau et al. [11][4]. Figure 5 (right) shows the GDOS measured on a powder of C_{60} and performed at the ILL on the spectrometers IN4C and IN1BeF. IN4C is a time of flight spectrometer installed on a thermal neutron source, and IN1BeF is a filter analyzer spectrometer installed on a hot source [13]. Both spectrometers have their best performance in complementary ranges of the spectrum, while having an area of overlap. They are perfectly complementary and allow the determination of density of states in a wide frequency range at very low temperatures. As we can see in Fig. 5, the GDOS spectrum contains a large number of peaks and extends up to 210 meV. It therefore covers a very broad field of energies as a consequence of the extremely strong C–C bond (one of the strongest chemical bonds in nature) and the low mass of carbon atoms. These spectra are compared with DFT calculations performed using the software *DMol3*. The calculations were done on an isolated molecule, and allow assigning the different modes. For example, the first mode located at 32 meV is the intramolecular mode Hg^1, which implies an elliptical deformation of the molecule.

We generally divide the spectrum of internal vibration modes of C_{60} into two categories: the "radial" band (30 meV $<$ E $<$ 110 meV) and the "tangential" one (115 meV $<$ E $<$ 200 meV), which contains vibrations involving deformations of the C–C bonds ("stretching"). The same division of the spectrum applies to graphite for frequencies above 30 meV, which translates the similarity of both systems regarding their local interactions.

It is important to note that the experimental spectra are in very good agreement with calculations, which justifies *a posteriori* the assumption of decoupling between internal and external degrees of freedom.

[4] Measurements had been reported earlier (1991) by K. Prassides [12] using the same instrument. The data were however of much worse quality due to the limited quality and quantity of the sample available at that time.

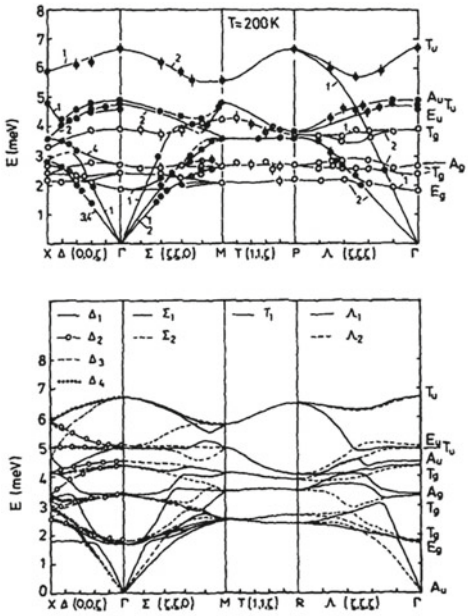

Fig. 6. *Top*: phonon dispersion curves measured at 200 K on a single crystal. – *Bottom*: theoretical phonon dispersion relations derived from a model built up from phenomenological force constants and accounting for van der Waals interactions between molecules. From reference [14].

Inter-molecular excitations in C_{60}

We focus now on the lattice dynamics of C_{60} within the phase known as *ordered*, appearing when the temperature drops below 260 K. Here, we will only consider the "external" modes – also called "inter-molecular" or "lattice" modes. To understand these lattice excitations in the ordered phase, it is necessary to provide an accurate description of the structure of this phase. Figure 4 shows a schematic configuration of C_{60} in the ordered phase with space group $Pa\bar{3}$.

In this phase, the C_{60} molecules are arranged in a simple cubic system. Although molecules are positioned at sites corresponding to a fcc mesh for indistinguishable molecules – like in the disordered phase – the unit cell becomes simple cubic when the C_{60} molecules become distinguishable. In the ordered phase, the C_{60} molecules can be oriented with two types of relative configurations: i) the configuration named "P" (as pentagon) where a double bond of a C_{60} faces a pentagon of the neighboring molecule, and ii) the configuration named "H" (as hexagon) where a double bond of a C_{60} faces a hexagon of the neighboring molecule. The result is a crystal lattice containing four non-equivalent C_{60} molecules. In this case, there are 24 degrees of freedom per unit cell (three rotations and 3 translations by molecule), resulting into 24 dispersion branches – including the 3 acoustic modes that can be measured on a single crystal using a 3-axis spectrometer.

The first measurements of the dispersion curve of the external modes were performed in 1992 on a single crystal of very small size (3 mm^3) by Pintchovius et al., on the 3-axis spectrometer 2T at the Laboratoire Léon Brillouin (Saclay, France) [15]. Focusing optics were used in order to allow measurements on this sample in a reasonable time. The experimental results are shown in Fig. 6, and are compared with calculations using a model accounting for intermolecular interactions [14].

Because of the degeneracy of some of these modes and of the imperfect resolution of the INS experiment, it is not possible to observe the 24 branches on the top of the

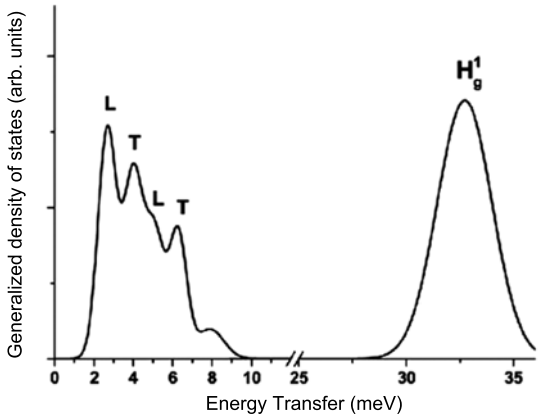

Fig. 7. GDOS of a C_{60} powder measured at room temperature on the IN4C spectrometer at the ILL. L and T refer to Libration and Translation features respectively.

Fig. 6. Some of these branches keep their translational character (the "phonons"), and some other keep their rotational character (the so-called "librations"). Some other modes possess a mixed character. It is possible to experimentally determine the character of each of these branches by playing with the dependence of the scattered intensity on the scattering vector associated with this mode (see ref. [16] for more details). It is also possible to observe anti-crossing phenomena between the branches, which indicates a coupling between some of the inter-molecular modes. Indeed, the mixture of characters of the modes indicates a coupling between the rotational and the translational degrees of freedom, and this coupling is in particular responsible for the contraction of the network upon orientational ordering [17]. These phenomena, as well as the general shape of the dispersion branches, are well reproduced by the model proposed by Pintschovius et al. [14].

The density of states of the external modes can be directly measured on a powder. Figure 7 shows the spectrum measured on the spectrometer IN4C in an energy range around the external modes. The first peak in the GDOS at 2.7 meV is attributed to the main component of the contribution of modes associated with librations. It should be noted that the dependency of the intensity of this mode with the scattering vector Q is characteristic of the rotational motion of C_{60}. The dynamical structure factor S(Q, ω) is shown in Fig. 8. Intense lobes are emerging at energy E $\simeq$ 2.5 meV and scattering vectors $Q = 3.5$ and $\sim 5.4\,\text{Å}^{-1}$. They correspond to the maxima of the form factor associated with the rotation of the C_{60} molecule [4,8,16,18]. Subsequently, we often call the peak at about 2.7 meV, "the" libration mode of C_{60}.

2.1.3 Effect of the order/disorder transition on the low frequency dynamics of C_{60}

The order-disorder phase transition is of first order type in C_{60}. Above 260 K, the molecules rotate almost freely[5]. This transition affects mostly the libration modes: the rotation loses its oscillatory (periodic fluctuation in time) character in favor of a diffusive character. In Fig. 9 the lobes in the spectrum $S(Q, \omega)$ are lost while an excess of intensity in the feet of the elastic line – called "quasi-elastic" (QE)

[5] We use the term "almost" in the sense that correlations of orientations between neighboring molecules actually exist. However, their characteristic time scale are so small that they can be neglected in a first approximation. Subsequently we will talk of "free rotations" and neglect any correlation of orientations between molecules in the disordered phase.

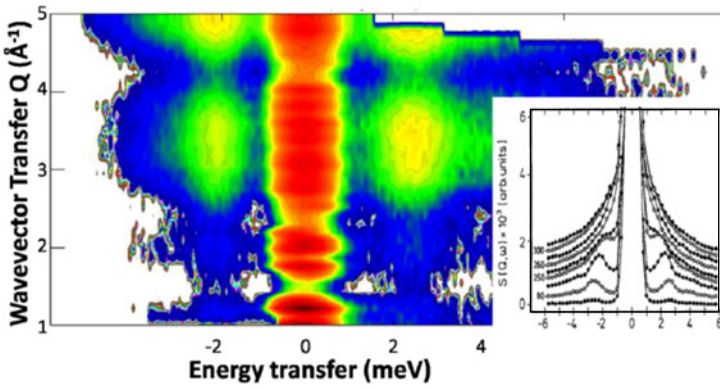

Fig. 8. Structure factor S(Q, ω) of C_{60} in the low frequency range, measured on IN4C in the ordered phase at T = 220 K. – *Bottom right*: Temperature dependence of the low-frequency rotation intensity (From [18]).

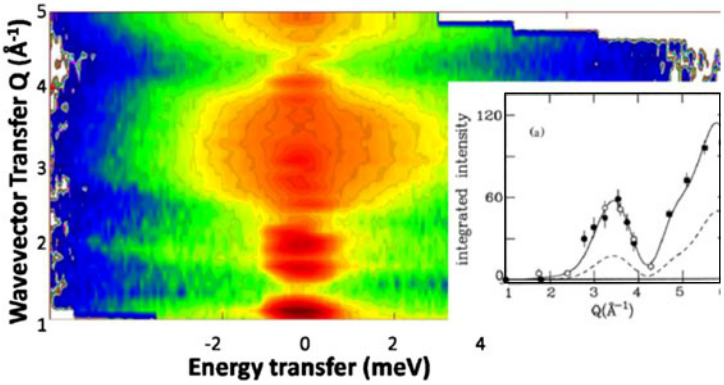

Fig. 9. Structure factor of C_{60} in the low frequency range, measured on IN4C in the disordered phase at T = 300 K – *Bottom right*: Temperature dependence of the integrated intensity of the quasi-elastic signal as a function of the scattering vector Q. The full line is the theoretical dependence for an isotropic rotation (from ref. [8]).

intensity – appears. The latter feature is associated with the diffusive nature of the rotational motion.

On the right of Fig. 8, one can observe that the QE signal, which is clearly visible for temperatures above 270 K, is sharpening upon cooling and gives rise to the libration peak for T < 255 K. The latter is separated from the elastic peak, and its position seems to progressively deviate from the central line as temperature drops. This apparent hardening close to the transition was first considered as an evidence for large anharmonicity of the rotational potential of fullerenes. Finally a more subtle effect was found to be at the origin of this observation. It is indeed linked to the temperature dependence of the proportion of C_{60} molecules in orientations P and H in the ordered phase [19], the frequency of the libration of the configuration P (the most stable) being larger than that of the configuration H.

The left side of Fig. 10 shows the temperature dependence of the relative occupancy of the crystal by C_{60} in the P configuration. These results were obtained by neutron diffraction at high resolution. One observes that this ratio increases continuously between 255 K and 90 K, and remains constant below 90 K. This discontinuity is reflected in the curve plotting the lattice parameter of the crystal as a function of temperature by a change in the slope of the thermal expansion of the crystal at 90 K

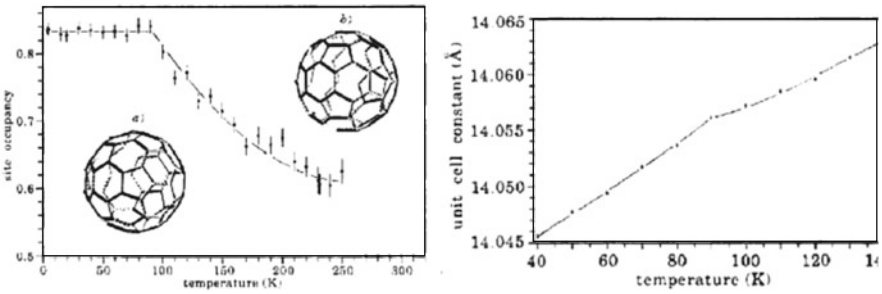

Fig. 10. *Left*: temperature dependence of the proportion of C_{60} molecules in orientation P (marked as (a)) with regards to those in orientation H. – *Right*: temperature dependence of the lattice parameter of a C_{60} crystal. From reference [20].

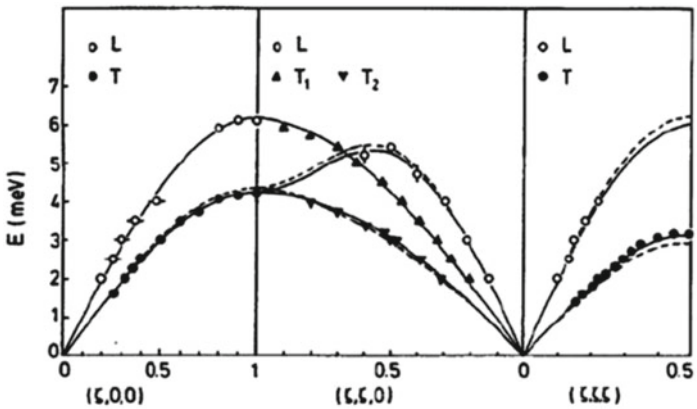

Fig. 11. Dispersion curves of the external modes of a single crystal of C_{60} in the disordered phase. Letters L and T indicate respectively the longitudinal and transverse branches. The full line results from calculations based on a force field model with three adjustable parameters. Dashed lines represent the dispersion curves of solid Krypton scaled to have a good match with those of C_{60}. (From [18].)

(Fig. 10 right). The reason for this discontinuity – which is also reflected in the evolution of the thermal conductivity of the material – is a new dynamic transition. Below 90 K, the jumps between P and H orientations are frozen, and the system evolves into a state called "orientational glass" where the proportion of C_{60} in P orientation remains blocked at 83.5%.

In the disordered phase, the loss of librational modes and the increase of the crystal symmetry (it is now in a face-centered cubic lattice $Fm\bar{3}$m) greatly simplifies the spectrum of the external modes. Indeed, there are only three degrees of freedom per molecule – those of rotation have disappeared – and one molecule per unit cell. The dispersion curves are reduced to three acoustic branches, as shown in Fig. 11. They can be modeled very accurately using a simple model where each C_{60} is considered as a noble gas atom. Each "meta-atoms" interacts with his neighbors through a force constant tensor having only three adjustable parameters [14,16].

2.2 Example of a molecular crystal with 2 patterns: The fullerene-cubane $C_{60} \cdot C_8H_8$ co-crystal

In 2005, a new type of material was synthesized on the basis of intercalated fullerenes: the fullerene-cubane co-crystal, in which cubane molecules (C_8H_8) are intercalated

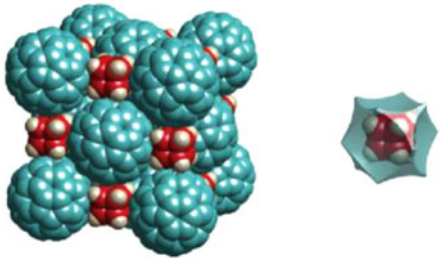

Fig. 12. Schematic representation of a crystal of fullerene-cubane (left) and detail of the shape of the inter-fullerene octahedral void around a cubane molecule. According to the reference [21].

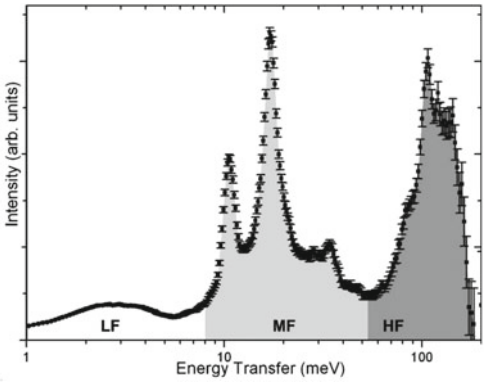

Fig. 13. Generalized density of states of a fullerene-cubane powder, measured on the spectrometer IN4C in the disordered phase. Areas LF, MF, HF locate the low frequency, intermediate frequency and high frequency ranges respectively.

inside the cubic lattice of C_{60} and are located on the octahedral sites (see Fig. 12). The lattice parameter of the resulting structure is expanded compared to that of C_{60}: 14.74 Å against 14.15 Å (at 300 K).

It is remarkable that the increase of the lattice parameter caused by the intercalation of cubane is lower than the lateral dimension of the cubane molecule. This reveals that the shape of the cubane molecule has some compatibility with that of the fullerene, enabling the guest molecule to be intimately mixed inside the host lattice.

Figure 13 shows the generalized density of states measured on the spectrometer IN4C at 300 K. The spectrum can be divided into three domains (LF, MF and HF), each associated with a certain type of dynamics. The molecules of cubane each comprise 8 hydrogen atoms. Therefore, the scattering cross section will be dominated by the strong incoherent contribution due to the cubane molecules. The most intense peaks of the spectrum are thus associated with the modes of these molecules.

The molecular modes of cubane have been studied by Yildirim et al. [22]: all the modes have their frequency located inside the HF band (except for the C-H stretching modes that are at higher frequencies) and form a very intense structure between 70 meV and 170 meV.

NMR experiments have shown that the C_{60} molecules exhibit orientational disorder at room temperature – equivalent to the disordered phase of pure C_{60} – while the cubane molecules remain frozen around well-defined orientations. This contrast in the dynamics of the molecules is at the origin of the epithet “rotor-stator” to describe the disordered phase.

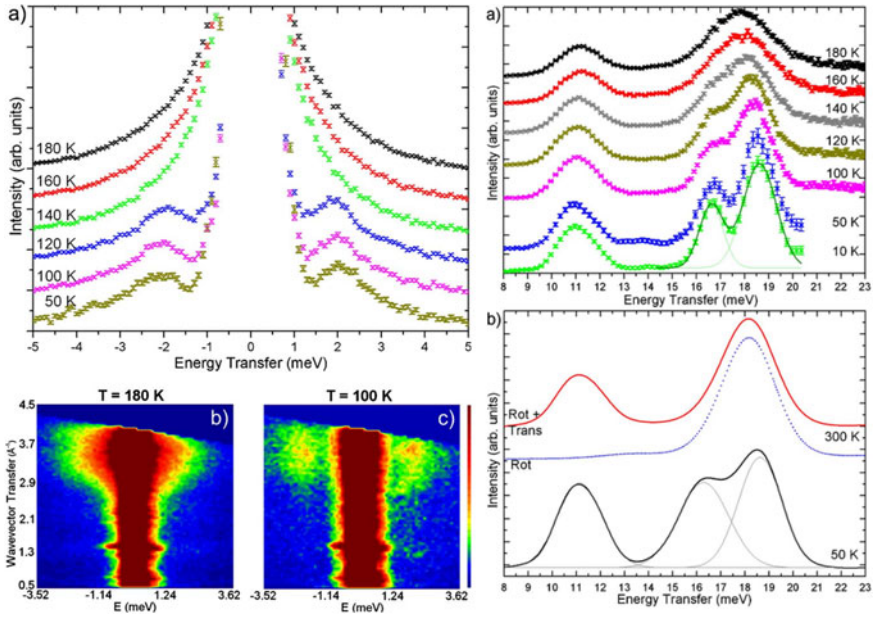

Fig. 14. *Left*: temperature dependence of $S(Q,\omega)$. a) Energy spectra for Q $\sim$ 3.3 Å^{-1} at different temperatures above and below the order-disorder transition (T_c = 140 K); b) and c) $S(Q,\omega)$ maps for T = 180 K (T > T_c) and T = 100 K (T < T_c) respectively. – *Right*: a) temperature evolution of the MF band, b) comparison between the experimental spectrum with the GDOS calculated by molecular dynamics simulations in the disordered (top) and ordered (bottom) phase respectively. The simulated spectra labeled "Rot + Trans" are calculated from rigid molecules taking into account the rotation and translation movements of the molecule. The spectra labeled "Rot" only takes into account the rotational movements in the analysis of the simulated trajectories (reproduced from [23]).

A structural transition to a less symmetrical orthorhombic phase, has been highlighted by X-ray diffraction at a temperature of 140 K [21]. Moreover, inelastic neutron scattering showed that the modes in the MF and LF bands are particularly affected by the transition. The free rotation of C_{60} is transformed into a libration below 140 K, whose frequency is ∼2.2 meV (see Fig. 14, Left), an observation in agreement with heat capacity measurements [24]. It should be noted that, unlike the case of pure C_{60}, the frequency of the libration of fullerenes is not observed to vary with temperature. This suggests that there is only one type of orientational arrangement in the ordered phase, or that such arrangements have very similar frequencies of libration.

The right side of Fig. 14 shows that the MF band has two contributions, whose intensities suggest that they are associated with the cubane molecules: a peak at 11 meV and one at 17.8 meV. By lowering the temperature below T_c, the latter feature splits into two contributions (16.5 meV and 18.5 meV) with an intensity ratio equal to 1/2.

The assignment of the different peaks was done by means of molecular dynamics simulations, which allowed to calculate the trajectories of the atoms with time. From these trajectories, one can deduce the neutron functions such as the generalized density of states[6]. In order to minimize the simulation time, it is also possible to consider the molecules as rigid bodies. The results from these simulations will thus only account for the external degrees of freedom of the molecules ("Rot + Trans" labeled

[6] Calculated from the Fourier transform of the velocities autocorrelation functions weighted by the scattering lengths of the atoms.

spectra on the right side of Fig. 14). In a second step, it is also possible to freeze the motion of the molecules' center of mass in the calculation of the neutron functions. In this case, we eliminate the contribution of the translations to the neutron spectrum, which allows us to isolate the peaks related to rotational vibrations ("Rot" labeled spectra on the right side of Fig. 14). Using this method, we could associate the feature at 17.8 meV to the three librations of cubane and the peak at 11 meV to the translational vibration of the cubane's center of mass.

In the disordered phase ($T > T_c$), the environment of a cubane molecule is isotropic as all the surrounding C_{60} molecules are equivalent. In this case, all three librations are degenerate and a single peak is observed in the spectrum (at 17.8 meV). When the temperature is lowered below the critical temperature T_c, this peak splits into two components resulting from symmetry breaking of the low temperature phase. The reported 1/2 intensity ratio of the two peaks in the doublet suggests that two spatial directions are equivalent.

The peak at 11 meV, by contrast to what is observed for the libration band, is not sensitive to the ordering of the lattice. This peak dominates the range of the phonon GDOS where the contributions of lattice modes – optical and acoustic – are expected.

The crystal of fullerene-cubane has a fcc structure at room temperature, and the pattern of the unit cell therefore contains one molecule of C_{60} (mass $M_{C_{60}} = 720$ amu) and one cubane molecule (mass $M_{C_8H_8} = 104$ amu). The phonon dispersion curves have six branches – three acoustic and three optical.

It is interesting to understand why the single peak at 11 meV dominates the spectrum in the energy range of phonons. Let us apply the formalism of neutron scattering to the case of fullerene cubane and express the one-phonon incoherent cross section [25]. We suppose that the crystal consists of two molecules ◯ and □, with respective masses $M_{\bigcirc} = M_{C_{60}}$ and $M_{\square} = M_{C_8H_8}$. We write their incoherent scattering cross sections $\sigma_{inc}(\bigcirc)$ and $\sigma_{inc}(\square)$, and we study the phonons of this molecular crystal $\{\bigcirc, \square\}$ assuming these molecules are rigid bodies (we omit their internal degrees of freedom). The one-phonon incoherent cross section can be written as:

$$\left(\frac{\partial^2\sigma}{\partial\Omega\partial E_f}\right)_{inc}^{1-ph(+)} = \frac{k_f}{k_i}\sum_{\kappa\in\{\bigcirc,\square\}}\frac{\sigma_{inc}(\kappa)}{8\pi M_\kappa}e^{-2W_\kappa(\boldsymbol{Q})} \times\sum_{j,\boldsymbol{k}}\frac{|\boldsymbol{Q}\cdot\boldsymbol{e}_j(\kappa|\boldsymbol{k})|^2}{\omega_j(\boldsymbol{k})}[1+n(\omega_j(\boldsymbol{k}))]\delta(\omega-\omega_j(\boldsymbol{k})).$$

In our case, $\sigma_{inc}(\bigcirc) = 0$ since the carbon incoherent cross section is negligible, which leads to:

$$\left(\frac{\partial^2\sigma}{\partial\Omega\partial E_f}\right)_{inc}^{1-ph(+)} = \frac{k_f}{k_i}\frac{\sigma_{inc}(\square)}{8\pi M_\square}e^{-2W_\square(\boldsymbol{Q})}\sum_{j,\boldsymbol{k}}\frac{|\boldsymbol{Q}\cdot\boldsymbol{e}_j(\square|\boldsymbol{k})|^2}{\omega_j(\boldsymbol{k})}[1+n(\omega_j(\boldsymbol{k}))]\delta(\omega-\omega_j(\boldsymbol{k})). \quad (2)$$

As illustrated in Fig. 15, in the case of a linear diatomic chain, the large mass difference between the two molecules is responsible for the very low dispersion of the optical modes which in turn contribute massively to the density of states. This mass difference is also responsible for the quasi-immobility of the light molecule (here the cubane) for the acoustic modes at the zone boundary (ZB): $\boldsymbol{e}_{ac}(\square|\boldsymbol{k}_{\in ZB})=0$. From Eq. (2) this implies that the intensity of the acoustic modes at the Brillouin zone boundary will be very weak in the spectrum of the GDOS. Therefore, the phonon spectrum of the fullerene-cubane will be dominated by a single contribution originating from intense optical modes. The non-dispersiveness of the optical modes is reminiscent to the contribution of "rattling" modes (vibrations in cages).

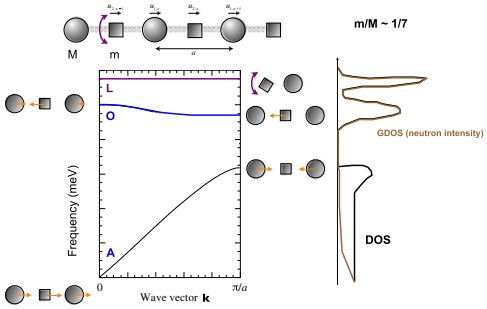

Fig. 15. *Top*: schematic view of the diatomic linear chain, a simple modelization of the fullerene-cubane co-crystal. *Left*: phonon dispersions of the acoustic (A), optical (O) and libration (L) modes. The displacement pattern of the modes at the zone center ($k = 0$) and edge ($k = \frac{\pi}{a}$) are represented beside. *Right*: the corresponding density of state (black full line) and the GDOS derived from equation 2 (brown full line). a is the unit cell parameter.

In conclusion, it appears clearly that the structural transition observed at $T_c = 140\,K$ is accompanied by a dynamic transition where the rotor-stator phase is lost. In the ordered phase the movements of rotation of the two types of molecules have an oscillatory character. This transition temperature is very low when compared to that of the crystalline phase of pure C_{60} (260 K). The system C_{60} is therefore highly lubricated by the presence of cubane molecules. This is due to the complementarity of their molecular shapes (concave and convex) which allows the molecules to overlap without blocking the fullerene rotation. The resulting expansion of the lattice prevents the adjacent C_{60} to feel the weak anisotropy of their electronic cloud, which results in a lower transition temperature for the order/disorder transition. Cubane molecules play the role of "molecular bearings" in the system.

3 Vibrations of a 2D-molecular and 1D-atomic crystal: Single-walled carbon nanotube bundles

3.1 A single-walled nanotube built from rolling up a graphene sheet

There are two main families of carbon nanotubes: single-walled carbon nanotubes (SWNT) and multi-walled carbon nanotubes (MWNT). SWNT can be considered as the result of winding a graphene sheet onto itself, in order to form a cylinder with a length of about 1 μm and a diameter in the nanometer scale. Depending on how the sheet is wound, it leads to different atomic structures (referred to as different helicity or chirality) having distinct electronic properties. One obtains either metallic or semiconducting nanotubes (for details, see for example Chapter 4 of [26]).

Regardless of how the graphene sheet is rolled up in a tube, it is always possible to define a 1D unit cell along the long axis of the nanotube[7], so that the SWNTs can be considered as one-dimensional crystals (see Fig. 16) to which we associate the adjective "atomic" because two adjacent cells are connected by covalent interactions.

The SWNT bundles may contain several dozen of tubes and are spontaneously formed as a result of inter-tube van der Waals forces. A planar section of a bundle perpendicular to the tubes long axis will show a centered hexagonal 2D lattice (see Fig. 16, right panel). No longitudinal correlation between two different tubes of the same bundle has ever been demonstrated, probably because bundles are formed

[7] We will call this direction the longitudinal axis.

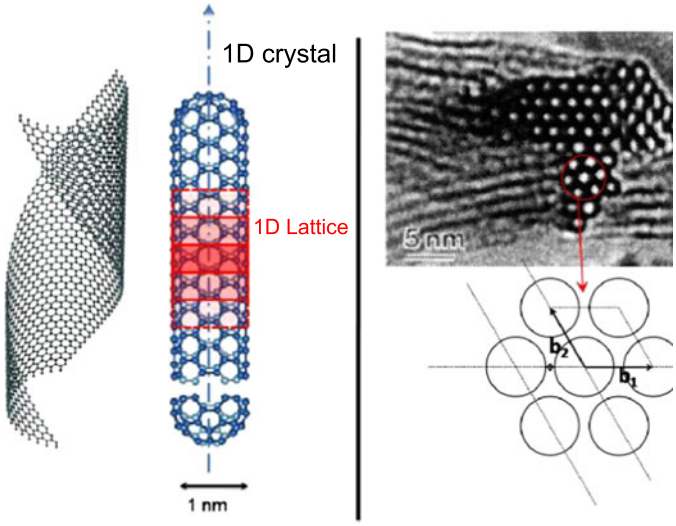

Fig. 16. *Left*: structure of a single-walled nanotube and definition of its unit cell – *Right*: bundle of parallel tubes and definition of the molecular 2D lattice (the electron microscopy image is taken from [27]).

with tubes of different helicities. This is why we call this system "1D-atomic" and "2D-molecular" depending on the studied direction.

3.2 Single-walled carbon nanotubes excitations

The one-dimensional unit cell of a carbon nanotube contains a number N, typically a few tens, of carbon atoms. The number of dispersion branches 3N along the longitudinal direction is therefore large, which would make their measurement very complex even if it was possible to synthesize single crystals.

For isolated tubes, four branches have zero frequency in the center of the Brillouin zone. These are the three acoustic modes (1L, 2T) and the rotation about the axis of the tube. Since the tubes self-organize into a bundle, the rotation becomes a low frequency libration which is one of the first optical modes of the system. The dispersion curves – and the density of states associated with them – calculated for a nanotube with a diameter of 14 Å, isolated and in bundle, are shown in Fig. 17.

The complexity of the dispersion curves of the isolated tube is reflected in the density of states by a very choppy profile. This translates the multitude of the 1D van Hove singularities – originating from the folding of the graphene branches – at the center and at the edge of the Brillouin zone of the tube[8]. At low frequency, the spectrum is dominated by radial modes which involve the deformation of the cylindrical shape of the tube. The frequency of these first optical modes can be very low, to a point where hybridization with the lattice modes is possible. Thus, unlike the case of C_{60}, it is not possible to make a clear distinction between lattice modes and molecular vibrations in the nanotubes. The most famous of these radial modes is the so called "radial breathing mode", of Hg symmetry and Raman active, and whose frequency is linearly related to the inverse of the diameter of the nanotube [29]. For tubes of diameter 14 Å, this mode is measured at ∼22 meV (a representation of this mode is given on Fig. 18).

[8] In a one-dimensional system, the contributions from the edge and from the center of the Brillouin zone are equal in number.

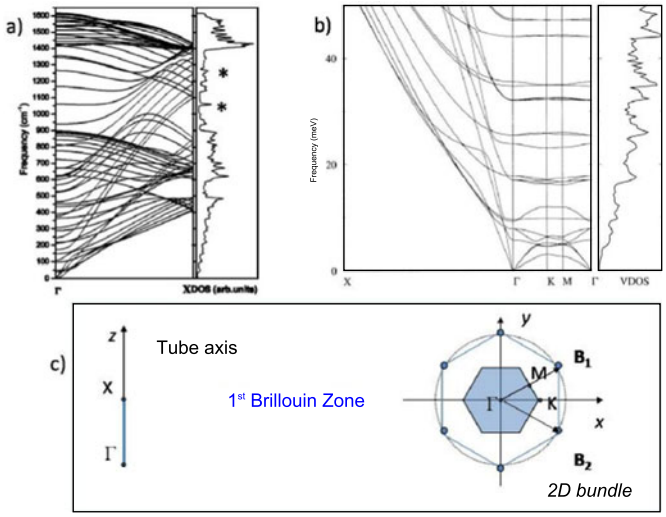

Fig. 17. a) Phonon dispersion curves of an isolated nanotube with diameter 14 Å(from ref. [28]) – b) Low frequency part of the phonon dispersion curves for a 14 Å diameter nanotube organized into bundles (from ref. [26]) – c) The first Brillouin zone of an isolated nanotube is a segment parallel to the longitudinal direction (Left), while it takes the forme of a cylinder with an hexagonal section in bundle (Right). Stars on figure a) indicate specific contributions of nanotubes which appear in the experimental spectra (see Fig. 18 curve c)).

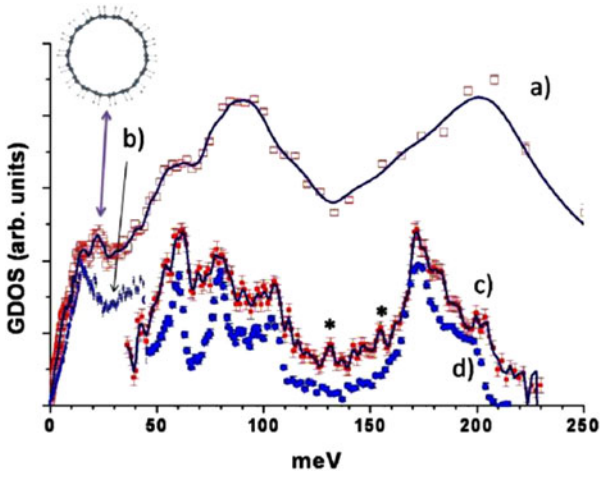

Fig. 18. a) Generalized density of states (GDOS) of a powder of single-walled carbon nanotubes with diameter 14 Å, measured on the IN6 spectrometer at 300 K and c) measured on the spectrometer IN1BeF at 10K – b) and d) The equivalent data for graphite. The stars indicate the van Hove singularities which can be the equivalent to those calculated in Fig. 17. The radial breathing mode (RBM) is shown. A peak at ~ 20 meV in the GDOS is assigned to this mode in agreement with the results of Raman spectroscopy performed on the same sample.

The study of the dynamics of carbon nanotubes by inelastic neutron scattering is more delicate than for fullerenes, since the samples exhibit a much lower crystallinity and a distribution of structural parameters (tube diameter, bundle sizes, purity, ...) that make data interpretation difficult. The most widely used technique for studying

these systems is by far Raman spectroscopy, which takes advantage of the resonant character of its cross section for photo-selecting a particular tube diameter in the sample [26]. The resonance is so powerful that it allows studying the spectral response of a single tube.

From the standpoint of atomic structure, a carbon nanotube is very close to a graphene sheet, and we can therefore expect that the density of states of a sample of carbon nanotubes has strong similarities with that of a sample of graphite. This is confirmed experimentally: Fig. 18 presents a comparison between the GDOS of these two types of samples (see also [30]). The density of states of SWNT results from the combination of data obtained on two spectrometers at the ILL (IN6 and IN1BeF).

One can note that experimental nanotube and graphite GDOS are actually very similar in the high frequency range, but small differences are nevertheless observed. First, in the spectra c) and d) of Fig. 18, small peaks are visible in the SWNT GDOS in the total frequency range, while they do not appear in the graphite GDOS. These peaks correspond to the 1D van Hove singularities and are located at frequencies characteristic of optical modes at the center and/or edge of the longitudinal Brillouin zone (along the nanotube axis). These contributions are particularly well reproduced by DFT calculations performed by Ye et al. [28] and shown in Fig. 17. Finally, the SWNT GDOS is larger than that of graphite in the range of energies below 40 meV. This excess reveals the presence of modes specific to carbon nanotubes, such as the RBM which is illustrated in Fig. 18. These modes are strongly dependent on the diameter of the tubes: they obviously do not have an equivalent in graphite.

The lattice "bundle" modes are very difficult to distinguish in the nanotube GDOS. Their hybridization with the first optical modes of the tubes, and the relatively small number of tubes per bundle makes their contribution to the GDOS large and difficult to isolate. They can be observed however in the lowest part of the spectrum ($E < 1.5$ meV), in the Debye range of the GDOS which is dominated by the contributions from acoustic modes. In this range, the GDOS is very sensitive to the dimensionality of the system (see [31]), and its linear dependence with frequency is characteristic of a two dimensional array. The latter observation is in agreement with the quadratic temperature dependence of the specific heat $C_P(T)$ for $T < 100$ K, measured on the same samples [32,33]. Figure 17(b) shows the dispersion curves of a bundle of nanotubes in the longitudinal ($\Gamma - X$) and transverse ($\Gamma - K - M - \Gamma$) directions . The slope of the acoustic modes in the longitudinal direction is very strong, their contribution to the density of states becoming negligible. In this region of the spectrum, the relevant lattice is therefore the two dimensional network resulting from the packing of tubes in bundles.

4 Carbon nanopeapods: C_{60} 1D chains confined inside single-walled carbon nanotubes

The last system we will study in this review is an inclusion compound of carbon nanotubes, where C_{60} fullerenes are inserted inside matching diameter SWNT ($\varnothing = 1.4$ nm), forming the so-called "peapods". These structures – first revealed by TEM – indeed recall the image of peas inside their pods (Fig. 19) and have thus been named that way.

As for fullerene and carbon nanotubes, the synthesis of the carbon nanopeapods was fortuitous – they were first observed in 1998 when looking at TEM images of a batch of laser ablation carbon nanotubes [34]. The passion triggered by their discovery was such that a year later a synthesis method was published [35] allowing the production of these objects in sufficient quantities for advanced studies. With the increasing control on the nanotube diameter, very high quality peapods could

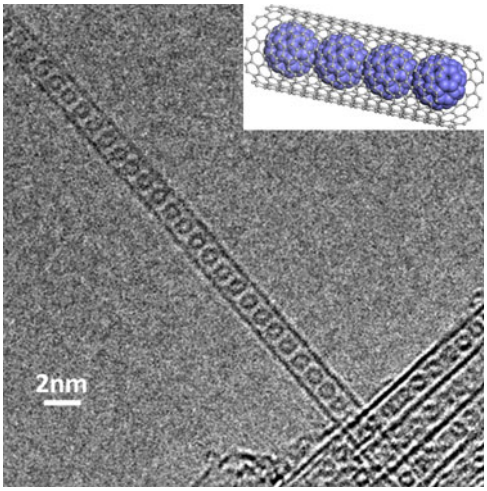

Fig. 19. Transmission Electronic Microscopy image of a C_{60} peapod sample. The inset shows a schematic representation of the molecular structure. TEM picture courtesy of Y. Niimi and K. Suenaga.

be produced [36] – *i.e.* high yield and filling rate, low impurities. Figure 19 shows a high resolution TEM image of one of those high quality samples. One can see that the filling rate appears very important. Most of the nanotubes gather into hexagonal bundles, which is confirmed by X-ray diffraction (XRD) [37].

One-dimensional (1D) systems are not only Nature curiosities, they are of fundamental interest as they provide physicists with models that are analytically solvable [38]. Despite their apparent simplicity, their ability to capture the essence of the physics at stake in more complex systems has given 1D systems a central role. However, actual 1D systems are not so common, especially when it comes to studying them on a wide temperature range. Nevertheless, the exceptional stability of the peapods (from 0 to 1100 K before further coalescence [39]) makes them a very good model 1D system, and it is quite interesting to study to what extent the 1D confinement of the C_{60} molecules can affect their dynamical properties. In this section, we will highlight the major results that were obtained using neutron scattering on the dynamics of these exotic objects.

In the peapods, the C_{60} represent only $\sim$30% of the total mass of the sample, the great majority being due to the carbon nanotubes. Thus, in order to extract experimental data regarding the sole C_{60}, one has to proceed by comparison with data obtained from empty nanotubes in the same conditions.

The generalized density of state (GDOS) of C_{60} peapods was measured at low temperature on the $[0, 200]$ meV energy range, using the thermal neutrons spectrometers IN4C (time of flight) and IN1BeF (triple axis) at the ILL. The results are shown on Fig. 20 where the GDOS of the peapods is compared to that of empty nanotubes and bulk C_{60}. In the range of C_{60} molecular mode, *i.e.* >30 meV, one can clearly see that the GDOS results from the weighted sum of the tubes' and of the fullerenes' contributions. In particular, in the domains where the tubes' contribution is weak ($E < 50$ meV and $E \in [110, 140]$ meV), the profile of the molecular modes of the C_{60} clearly arises as well defined peaks, like the H_g^1 mode at 33 meV. This indicates a weak coupling between the tubes and the C_{60} molecules.

The temperature evolution of the first molecular modes of the C_{60} is particularly interesting (Fig. 20 left). It shows indeed the progressive disappearing of their contribution as the temperature is increased above 100 K. This effect can be understood if

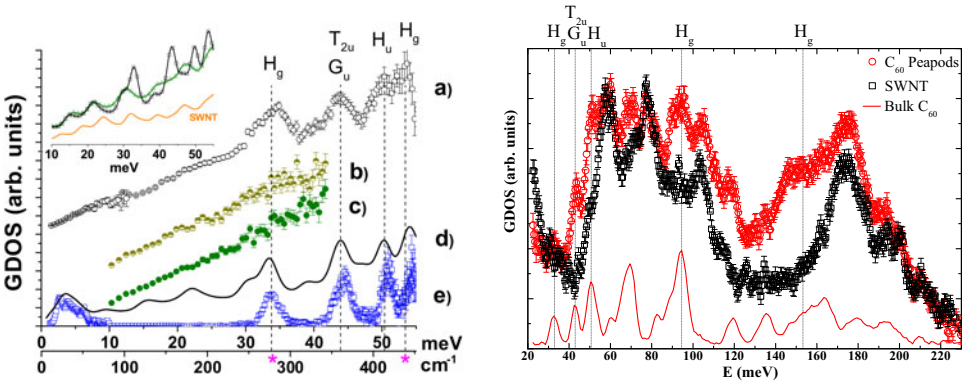

Fig. 20. *Left*: generalized density of states of the peapod sample measured on the IN4C spectrometer at 10 K (a), 150 K (b), 300 K (c), and the one calculated using the model developed in ref. [41] (d). The GDOS of a bulk C_{60} sample measured at 10 K (e) is also shown for comparison. *Inset*: the GDOS calculated for a peapod model (squares and triangles) and for a SWNT model (full line labeled "SWNT"). The GDOS were convoluted by a Gaussian function (2 meV FWHM) to simulate the instrument resolution. The curve with triangles symbols has moreover its contribution originating from the C_{60} vibrations further folded with a lorentzian function of 6 meV FWHM to account for the effect of the C_{60} rotations. From ref. [41]. *Right*: generalized density of states of the C_{60} peapod sample (circles) and of the SWNT sample (squares) measured at 10 K using the IN1BeF spectrometer (normalized to the mass of tubes), compared to the bulk C_{60} one (full line).

one recalls that these modes are convoluted by a function taking into account degrees of freedom of rotation and translation of the whole C_{60} molecule. Schematically, if one supposes that the rotation of the C_{60} molecule is independent of its internal degrees of freedom (atomic vibrations of the surface carbon atoms), the diffusion function writes:

$$S(\boldsymbol{Q},\omega) = S^{rot}(\boldsymbol{Q},\omega) \otimes S^{vib}(\boldsymbol{Q},\omega) \tag{3}$$

$$S(\boldsymbol{Q},\omega) = S^{rot}(\boldsymbol{Q},\omega) \otimes \left[S^{vib}_{el}(\boldsymbol{Q})\,\delta(\omega) + S^{vib}_{inel}(\boldsymbol{Q},\omega)\right] \tag{4}$$

$$S(\boldsymbol{Q},\omega) = S^{rot}(\boldsymbol{Q},\omega).S^{vib}_{el}(\boldsymbol{Q}) + S^{rot}(\boldsymbol{Q},\omega) \otimes S^{vib}_{inel}(\boldsymbol{Q},\omega) \tag{5}$$

where $S^{rot}(\boldsymbol{Q},\omega)$ and $S^{vib}(\boldsymbol{Q},\omega)$ are the dynamical structure factors associated with the rotation of the molecule as a rigid entity, and the atomic internal vibrations, respectively. The indices *el* and *inel* refer to the elastic and the inelastic parts of the diffusion function. If the rotation takes a relaxation character, its diffusion function becomes the sum of a certain amount of lorentzian functions whose widths are characteristic of the relaxation times at stake. The $S^{vib}_{inel}(\boldsymbol{Q},\omega)$ function being the sum of $\delta(\omega-\omega_j)$ [40], the GDOS spectrum will be formed of lorentzian functions centered at the frequencies of the molecular modes:

$$GDOS(\boldsymbol{Q},\omega) \propto \sum_j S^{rot}(\boldsymbol{Q},\omega-\omega_j)$$

$$GDOS(\boldsymbol{Q},\omega) \propto \sum_j \frac{\Gamma}{(\omega-\omega_j)^2+\Gamma^2}$$

the width Γ of the lorentzians being proportional to the inverse of the relaxation time, which will result in the enlargement of the fast molecular modes in the spectrum. In the peapods, this dynamical disorder arises from the rotations of the C_{60}

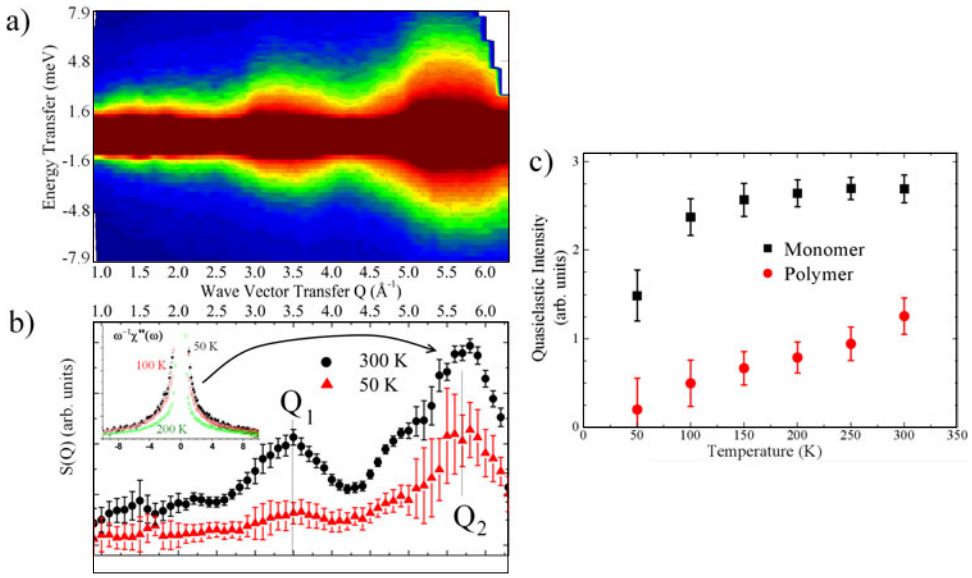

Fig. 21. Evolution of the fullerenes' rotational dynamics. a) $S(Q,\omega)$ map taken at 300 K on IN4C on a monomer C_{60} peapod sample, for incident wavelength of 1.7 Å. Maximum intensity is saturated for clarity. – b) Corresponding energy integrated $S(Q)$ at 300 and 50 K. The inset shows the susceptibility in $Q_2 = 5.4\,\text{Å}^{-1}$ at 200, 100 and 50 K (resp. green triangles, red circles and black squares) – c) Comparison of the total quasi-elastic intensity scattered by monomer (squares) and polymer (circles) samples (both normalized to C_{60} mass in the sample).

molecules. Indeed, a quasi-elastic signal is clearly observed in the spectra, with a width $\Gamma \simeq 6$ meV at room temperature. The Q dependence of this signal (energy integration of the $S(Q,\omega)$ map shown Fig. 21(a)) is represented Fig. 21(b): its shape is identical to that of bulk C_{60} shown Fig. 9. However, the temperature dependence of the signal arising from the rotations of the C_{60} is extremely different when the molecules are confined in 1D. Indeed, contrary to the case of bulk C_{60}, no clear signal of the freezing of the rotations can be observed in the peapods as no libration peak appears even at temperatures as low as 1.8 K [41]. Nevertheless, the susceptibility measured around the second peak (in $Q_2 = 5.4\,\text{Å}^{-1}$) does show a jump between 200 and 100 K. This is characteristic of the loss of the quasi-elastic signal in this temperature range, and it reveals a strong modification of the rotational dynamics, from a diffusive character towards a libration type. More information arises from the analysis of the total intensity of this quasi-elastic signal. Indeed, if the motion that animates the C_{60} is diffusive, the total quasi-elastic intensity is an indicator of the disorder within the sample – in broad outline, the more important the disorder, the higher the intensity – and the signal's intensity should not depend on the temperature. However, if this motion becomes vibrational, the signal turns into a density of state of phonons (or librons in that case), whose intensity depends on the temperature following a Bose distribution, *i.e.* linearly for $k_B T \gg \hbar\omega$.

Besides, let us recall that it is possible to polymerize the C_{60} chains by means of high pressure and high temperature [42,43]. In that case, all the C_{60} molecules within the nanotubes are bound to their two neighbors by $2+2$ cycloaddition between two facing double bonds. The polymerization of our peapods samples was performed by V. Davydov and V. Agafonov, by pressing the monomer sample at 25 kbar at 280 °C during 30 min.

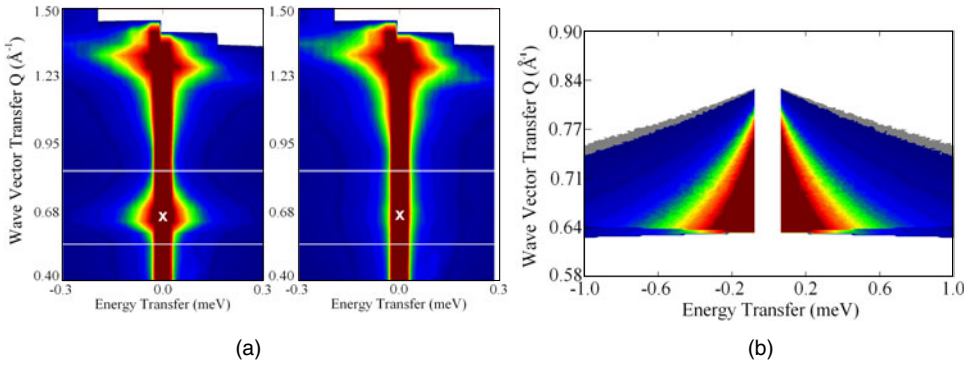

Fig. 22. a) Obtaining of the 1D acoustic phonons' density of states: $S(Q,\omega)$ maps taken at 420 K on IN5, for incident wave length of 8 Å, in the parallel (left) and orthogonal (right) configurations. Maximum intensity is saturated for clarity. The white cross indicates the location of the signal from the C_{60} translational motions, around the wave-vector position corresponding to the first C_{60} chains correlation peak at 0.64 $Å^{-1}$. The white horizontal lines mark the Q range of interest, range on which the signal is integrated to obtain Fig. 24(a). – b) Simulated dynamical structure factor $S(Q,\omega)$ in the case of a pellet of C_{60} peapods with crystalline C_{60} chains observed on a TOF instrument.

The resulting evolution of the quasi-elastic intensity (QEI) for both monomer and polymer samples is shown in Fig. 21(c). The evolutions are clearly different in the two samples, which reflects the great difference in their rotational dynamics. For the polymer, the QEI is linear with the temperature, which reflects a bosonic behavior. In the case of the monomers, the QEI remains constant above ∼200 K and decreases under this temperature. Moreover, the QEI of the monomer is always above that of the polymer – when normalized to the mass of C_{60} in the samples, which reflects the higher orientational disorder in the monomer sample.

As a consequence, it is clear that whereas the polymerized chains show a librational dynamics at all studied temperatures, the monomer chains show an isotropic rotational diffusion at high temperature. This diffusive motion then progressively turns into a librational behavior below 200 K, with a progressive ordering of the orientations of the libration axis.

However, since the C_{60} chains can be assimilated to a model 1D system in which no phase transition is expected, one may wonder what is the cause to this orientational ordering of the monomer fullerenes chains. The answer lies in the translational dynamics of the molecules.

In order to monitor the translational dynamics of the C_{60} with INS, one needs again to distinguish the signal from the tubes and the one from the C_{60} chains. This can be done by the use of an oriented sample: by pressing the buckypapers into pellets, one obtains a rather good "2D powder", the tubes being mainly oriented along the plane of the pellets (with an off-plane distribution of $\pm 25°$ in our samples). Let us recall that the dynamical structure factor $S(Q,\omega)$ is proportional to $(\boldsymbol{Q}\cdot\boldsymbol{e}_p)^2$, where $\boldsymbol{Q}$ is the neutron transfer vector and $\boldsymbol{e}_p$ is the direction of the motion of the molecules induced by the phonon p. Thus, the use of two configurations, referred to as "para" and "ortho" in the following, will allow us to separate the response from the C_{60} chains from the one of the nanotubes. These two configurations respectively correspond to the cases in which the plane of the pellet is set either parallel or orthogonal to the transfer vector $\boldsymbol{Q}$ corresponding to the elastic scattering of the inter C_{60} distance. The result is that the longitudinal C_{60} 1D phonons contribution is maximal in the para configuration (around 0.64 $Å^{-1}$ [51]), and is extinguished in the ortho one, as can clearly be seen in Fig. 22(a) showing the $S(Q,\omega)$ maps taken on IN5

at 420 K in both configurations. The inelastic contribution of the tubes is much less sensitive to the orientation in this $[Q, \omega]$ range. Indeed, in this area it consists mainly of soft radial modes and, since the motion of the atoms is perpendicular to the axes of the tubes, atomic displacements occur in all three directions of space, and thus their contribution is similar in both configurations. The above considerations allow us to extract the inelastic contribution of the fullerenes chains by a simple subtraction of the para and the ortho data – the same treatment is applied to the polymer sample.

Let us finally note that, due to the geometry of a neutron time of flight instrument, the sample will only be parallel (resp. orthogonal) to the wave vector $\boldsymbol{Q}$ for $Q_0 = 0.64\,\text{Å}^{-1}$ and $\omega = 0$ – where $Q_0 = 2\pi/L$ is the first diffraction peak from the fullerene chain, L being the mean inter-fullerene distance. For the second diffraction order, $\boldsymbol{Q}$ and the sample make similar angles (about 15° difference) in both configurations, resulting in an almost unchanged feature around $Q = 2\,Q_0 = 1.28\,\text{Å}^{-1}$. In the following, we will consider only the region where Q belongs to $[0.5, 0.8]\,\text{Å}^{-1}$ and ω stays within $[-0.5, 0.5]$ meV in order to monitor the most parallel and the most orthogonal configurations (area selected by the white lines on Fig. 22(a)).

The temperature evolution of the susceptibility $\chi''(\omega)/\omega$ integrated over $Q \in [0.5, 0.8]\ \text{Å}^{-1}$ for the monomer is shown Fig. 24(a). Two temperature ranges can be distinguished: the low temperature one (LT, $T \leq 200$ K), where the susceptibility varies with T, and the high temperature one (HT, $T \geq 260$ K), where the susceptibility is independent of the temperature.

The first image that comes to mind when modeling the long chains of C_{60} molecules is the very simple one of the *infinite* harmonic chain. In that case, no long range order can establish due to the cumulative thermal fluctuations, resulting in an unusual susceptibility that should depend on the temperature as $\chi''(\omega) \propto \frac{1}{(\omega/c)^2+T^2}$ [44,45]. Moreover, the scattered intensity should be of purely inelastic nature. However, this is not the case in either temperature ranges, where an elastic intensity is always observed and the temperature evolution does not fit. In fact, the chains behave at HT not as an *infinite* liquid harmonic chain but as a *finite* harmonic crystal – which explains the independence of the susceptibility on T as well as the presence of elastic intensity. The signal observed around Q_0 and $\omega = 0$ is not a quasi-elastic one but is the density of states of the acoustic phonons of the 1D finite chains. It appears as a quasi-elastic signal because it is averaged due to both the 2D orientation of the sample and the time of flight instrument geometry. This signal is well reproduced by simulations of 1D crystalline chains presented as a pellet with an instrumental resolution (Fig. 22(b)).

Moreover, another interesting feature of this signal is that its intensity is proportional to $1/c$, where c is the speed of sound in the 1D crystal (Fig. 23(a)) – $1/c$ is indeed exactly the density of state in the elastic approximation. As a matter of fact, the dynamical structure factors from the monomer and the polymer peapods samples – normalized to the mass of C_{60} and to the structure factor [37] differ only by a scaling factor of 1.7 (Fig. 23(b)). This means that the two systems are well modeled by the harmonic crystal model, and that $c_p = 1.7 \times c_m$, where c_p and c_m are the speeds of sound in the polymer and the monomer, respectively. Fortunately, the speed of sound in 1D polymer orthorhombic C_{60} is known ($c_p = 6.0\,\text{km.s}^{-1}$ [46]), which yields $c_m = 3.5 \pm 0.5\,\text{km.s}^{-1}$. This speed of sound is significantly higher – aside from the rather high uncertainty – from the one in bulk C_{60} ($c_{bulk} = 3.27 \pm 0.07\,\text{km.s}^{-1}$ [46]), which is in good agreement with the observed shorter inter-C_{60} distance that may be induced by a stronger intermolecular potential in C_{60} peapods, the origin of which is still to be understood.

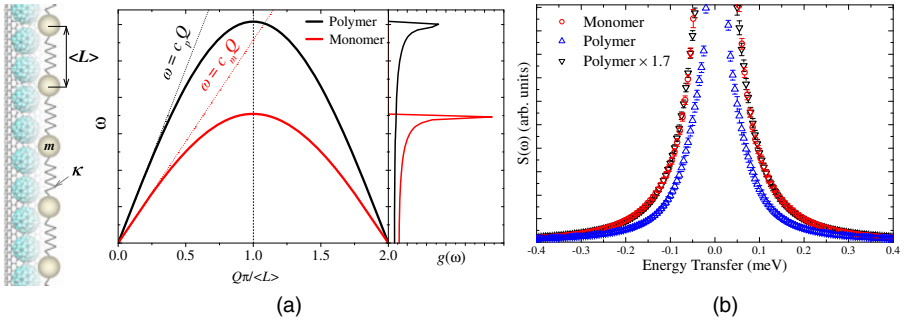

Fig. 23. a) Dispersion curves for an harmonic crystalline chain of masses m with two different spring constants κ, linked to the speed of sound c by $c = \sqrt{\kappa/m}$. The corresponding phonon densities of state $g(\omega)$ are shown on the right: at the lowest frequencies, their ratio scales like c_p/c_m. – b) Comparison of the experimental dynamical structure factor $S(\omega)$ for the monomer and the polymer peapods C_{60}. The data are normalized to the C_{60} mass in the different samples and to the intensity coming from the structure factor. There is only a scaling factor of 1.7 between the two $S(\omega)$, which corresponds to the ratio between the speed of sound in the two samples.

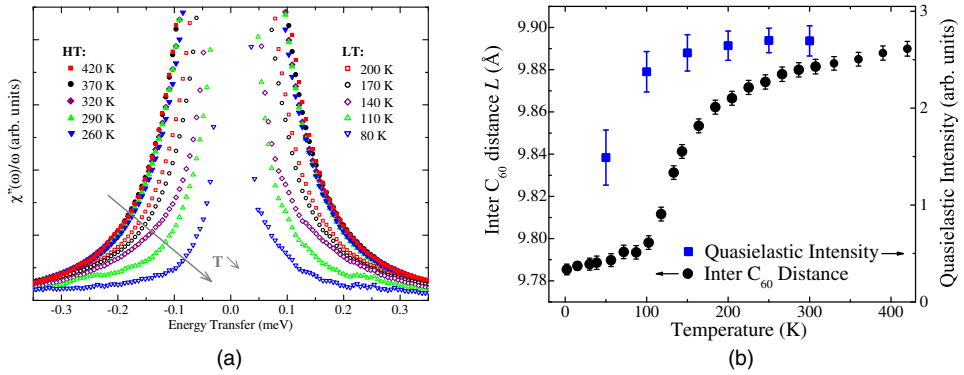

Fig. 24. a) Temperature evolution of the susceptibility $\chi''(\omega)/\omega$ of the quasi-elastic signal. Two behaviors can be distinguished: a high temperature one (HT – full signs) where the susceptibility is independent of the temperature, and a low temperature one (LT – empty signs) where the susceptibility is temperature dependent. Error bars are not represented for the sake of clarity. – b) Visualization of the effects of the rotation/translation coupling. (Circles, left axis) Temperature evolution of the inter-C_{60} distance $\langle L \rangle$ as measured on D16 at the ILL. (Squares, right axis) Temperature evolution of the quasi-elastic intensity for the monomer sample. The rapid contraction of the chains is correlated with the decrease of the fullerenes' orientational disorder.

Going back to the low temperature transition, one can see on Fig. 24 that the orientational ordering discussed above is coupled with a 1% contraction of the inter-C_{60} distance (Fig. 24(b)) together with the appearance of a soft dynamics – characterized by the transfer of the inelastic intensity into an elastic one (Fig. 24(a)).

These features could be explained by different effects. It has indeed been predicted that the weak interaction between fullerenes molecules in parallel chains inside a bundle would induce a 3D ordering of the 1D chains [47,48], resulting in a quite unusual second order solidification. Such a transition would indeed translate into the appearance of a soft mode (displacive transition), and the rotation/translation coupling would induce the contraction and the orientational ordering. Another possibility

would be that the chains start to feel some friction coming from the tube, which would result in the overdamping of the acoustic modes. The last possibility is that the rotation/translation coupling itself would become dominant at low temperature [49,50], which would induce this transition. More experimental data on the translational dynamics of the polymerized chains are yet necessary in order to fully understand this ordering transition.

5 Conclusion

In this review, we gave an insight of what neutron scattering has brought to the study of the dynamics of these original compounds that are the fullerenes and the carbon nanotubes. We described the major characteristics of the intra and inter-molecular excitations in these compounds as a function of temperature. We have then shown the evolution of the spectra and of the dynamics of these systems when cubane molecules are intercalated in the octahedral sites of the C_{60} lattice, or when fullerenes are confined on a 1D lattice inside the carbon nanotubes – hence forming the peapods. We saw that the temperature of the order-disorder transition can shift depending on the molecular environment of the C_{60}. Due to space restrictions, we had to leave apart other studies of C_{70} fullerenes and peapods, high pressure studies, alkali doped fullerenes, etc... For the same reasons, we barely evoked other experimental studies (x-ray diffraction, Raman spectroscopy, NMR, ...) that also brought important results on the structure and dynamics of fullerenes and nanotubes. We hope to have raised the curiosity of the readers and to have given some of them the desire to continue these studies.

Stéphane Rols and Helmut Schober are physicists and instrument scientists at the Institute Laue Langevin (ILL) in Grenoble (France). They are involved in the major part of the studies described in this paper, resulting from an active collaboration with Pascale Launois, physicist at the Laboratoire de Physique des Solides (LPS) at the University of Orsay (France), and Jean-Louis Sauvajol, physicist at the Laboratoire Charles Coulomb (L2C) at the University of Montpellier (France). Colin Bousige is finishing his PhD at the time of writing. He was involved into the synthesis and studies of the dynamics of the peapods and of the fullerene-cubane co-crystal, under the supervision of PL and SR. Julien Cambedouzou is assistant professor at the École Nationale Supérieure de Chimie de Montpellier (Montpellier, France) and was a former member of PL's team. He participated to the determination of the structure of the peapods samples and was involved into the first inelastic neutron measurements on these samples. Vyacheslav Agafonov is Professor at the University of Tours. He is involved into the X-ray and Raman characterization of the high pressure, high temperature (HPHT) transformed phase of the carbon peapods. Valery Davydov is a scientist at the Troisk center for high pressure research. He was the responsible of the HPHT treatment to the peapods leading to the polymeric phase of the confined C_{60} chain. Jacques Ollivier is physicist and instrument scientists at the ILL. He is involved into the inelastic neutron scattering experiments on the IN5 instrument. SR, CB and JC wrote the paper. The authors are indebted to Robert Almairac and Laurent Alvarez (L2C) for their investment in the XRD and Raman studies of carbon nanotubes, fullerenes and peapods. We also thank Hiromichi Kataura (National Institute of Advanced Industrial Science and Technology, Tsukuba, Japan) on one hand, and Sandor Pekker and Éva Kováts on the other hand for kindly providing us with samples of peapods and fullerene-cubane respectively. John Stride (University of New South Wales, Sydney, Australia), Jean-Marc Zanotti (Laboratoire Léon Brillouin, France), and late José Dianoux (ILL) were of considerable assistance in the experiments of inelastic neutron scattering and in the analysis of the neutron data. We also thank Mark Johnson and Éric Pellegrini (ILL) for their help during the preparation of numerical simulations and in the exploitation of trajectories from molecular dynamics simulations.

We wish to thank the Institute Laue Langevin for the beam time allocated and for the support to these studies.

References

1. H.W. Kroto, et al., Nature **318**, 163 (1985)
2. S. Iijima, Nature **354**, 56 (1991)
3. V.A. Davydov, et al., Phys. Rev. B **61**, 1936 (2000)
4. J.R.D. Copley, Neutron News **4**, 20 (1993)
5. P. Launois, et al., Int. J. Mod. Phys. B **13**, 253 (1999)
6. R. Tycko, et al., Phys. Rev. Lett. **67**, 1886 (1991)
7. P. Launois, et al., Phys. Rev. B **52**, 5414 (1995)
8. D.A. Neumann, et al., Phys. Rev. Lett. **67**, 3808 (1991)
9. J. Yu, et al., App. Phys. Lett. **63**, 3152 (1993)
10. R.L. Capelletti, et al., Phys. Rev. Lett. **66**, 3261 (1991)
11. C. Coulombeau, et al., J. Phys. Chem. **96**, 22 (1992)
12. K. Prassides, et al., Chem. Phys. Lett. **187**, 455 (1991)
13. `http://www.ill.eu/fileadmin/users_files/Other_Sites/YellowBook2008CDRom/index.htm`
14. L. Pintschovius, S.L. Chaplot, Z. Phys. B **98**, 527 (1995)
15. L. Pintschovius, et al., Phys. Rev. Lett. **69**, 2662 (1992)
16. L. Pintschovius, et al., Rep. Prog. Phys. **59**, 473 (1996)
17. D. Lamoen and K.H. Michel. Phys. Rev. B **48**, 807 (1993)
18. B. Renker, et al., Z. Phys. B **90**, 325 (1993)
19. H. Schober, et al., Phys. Rev. B **59**, 3287 (1999)
20. W.I.F. David, et al., Europhys. Lett. **18**, 219 (1992)
21. S. Pekker, et al., Nature Mat. **4**, 764 (2005)
22. T. Yildirim, et al., Chem. Phys. Lett. **309**, 234 (1999)
23. C. Bousige, et al., Phys. Rev. B **82**, 195413 (2010)
24. N. M. Nemes, et al., J. Phys. Chem. B **113**, 2042 (2008)
25. W. Marshall, *Theory of Thermal Neutron Scattering* (Clarendon Press, 1971)
26. A. Loiseau, P. Launois, et al., Understanding Carbon Nanotubes Lect. Notes Phys. 677, (2006)
27. L. Henrard, et al., Eur. Phys. J. B **13**, 661 (1999)
28. L.-H. Ye, et al., Phys. Rev. B **69**, 235409 (2004)
29. S. Rols, et al., eur. Phys. J. B **18**, 201 (2000)
30. S. Rols, et al., Phys. Rev. Lett. **85**, 5222 (2000)
31. J.-L. Sauvajol, et al., Carbon **40**, 1697 (2002)
32. J.C. Lasjaunias, et al., Phys. Rev. Lett. **91**, 25901 (2003)
33. J.C. Lasjaunias. C.R. Physique **4**, 1047 (2003)
34. B.W. Smith, et al., Nature **396**, 323(1998)
35. B. Burteau, et al., Chem. Phys. Lett. **310**, 21 (1999)
36. H. Kataura, et al., Synth. Met. **121**, 11951196 (2001)
37. J. Cambedouzou, et al., Eur. J. B **42**, 31 (2004)
38. E.H. Lieb, D.C. Mattis, *Mathematical physics in one dimension: exactly soluble models of interacting particles* (Academic Press, 1966)
39. S. Bandow, et al., Chem. Phys. Lett. **337**, 48 (2001)
40. G.L. Squires, *Thermal neutron scattering* (Cambridge University Press, Cambridge, 1978)
41. S. Rols, et al., Phys. Rev. Lett. **101**, 65507 (2008)
42. S. Kawasaki, et al., Carbon **43**, 37 (2005)
43. M. Chorro, et al., Phys. Rev. B **74**, 205425 (2006)
44. V.J. Emery, J.D. Axe, Phys. Rev. Lett. **40**, 1507 (1978)
45. I.U. Heilmann, et al., Phys. Rev. B **20**, 751 (1979)

46. Y.M. Soifer, et al., J. Al. Comp. **310**, 292 (2000)
47. C. Carraro. Phys. Rev. B **61**, 16351 (2000)
48. M. Mercedes Calbi, et al., Phys. Rev. B **67**, 205417 (2003)
49. K.H. Michel, et al., Phys. Rev. Lett. **95**, 185506 (2005)
50. K.H. Michel, et al., Eur. Phys. J. B **48**, 113 (2005)
51. C. Bousige, et al. (submitted)